

Fundamentals of the Near-Source Problem

John F. Hall and Brad T. Aagaard
California Institute of Technology

June 1998

1 Ground Motion

Near-source ground motions are rapid ground displacements associated with the shear wave which propagates ahead of the rupturing fault. Considering the capacity of existing bridges, ground displacements of a half a meter taking place at rate of a meter per second would be of concern, and near-source motions from even moderate earthquakes may easily reach these amplitudes. Larger earthquakes efficiently produce even larger ground displacements; several meters are certainly possible at many sites in California. The primary aspects of near-source effects are summarized below; a more complete description with references is presented in [1].

The mechanism by which near-source ground motions are generated stems from the fault rupture process. Inversion studies of actual earthquakes have indicated that slip on the fault involves only a small portion of the fault at any given time, within which rapid slip occurs, and this region of slipping propagates along the fault. Such a process efficiently generates shear waves; the propagating rupture continually reinforces the shear wave traveling just ahead, causing it to build in amplitude. The shear wave motion is perpendicular to the fault, and in the case of a strike-slip fault, this motion is horizontal. Because there is little residual displacement in the direction normal to a fault, the near-source displacement must contain a reversing phase. Large displacements may also occur in the fault-parallel direction and are associated with the permanent offset on the fault. Compared to the fault-normal motion, the parallel motion probably occurs more slowly, and since there is no reversing phase, it will be less damaging in general. These features also apply to inclined faults except, in these cases, the fault-normal motion has a large vertical component; however, as the near-source shear wave approaches the ground surface, it travels through softer rock and soil where it bends around toward the horizontal due to refraction. The reversing phase is still present.

Directivity is associated with near-source ground motion by the very nature of the generating mechanism. Only sites in the direction toward which the fault rupture is propagating will see the amplitude building effects. Nevertheless, while directivity spares some significant portion of the near-fault region, the region seriously affected can still be considerable [1].

The near-source waveform depends on details of the rupture history. Two important parameters include the speed at which the slip takes place and the velocity at which the rupturing zone propagates along the fault. The former translates into more rapid ground motion, while the latter, which is bounded from above by the local shear wave speed, affects the rate of reinforcement of the shear wave traveling ahead of the rupture. As the velocity of rupture propagation approaches the shear wave speed, the amplitude of the near-source shear wave grows rapidly. Fault rupture may also be irregular with starts, stops, and nonuniform spatial distributions of slip, all of which affect the waveform at all periods. Unfortunately, there is not nearly enough recorded data on near-source effects, especially from large earthquakes. Some evidence, such as the Lucerne record from the

1993 M_W 7.2 Landers earthquake [2], suggests that a single large displacement pulse dominates the near-source ground motions from large earthquakes.

To partially compensate for the lack of near-source data, for a number of years seismologists have been developing techniques to numerically simulate earthquakes ([3, 4, 5]). The more general procedures employ very large finite difference grids or finite element meshes with a slip history prescribed at each point of the fault. Simulations in which the fault slips by itself [6] are in the early stages of research. While these latest attempts avoid having to prescribe the slip, they rely on a friction law, and this is a subject about which there is much debate but little data on what is appropriate.

Results of a finite element simulation of a thrust earthquake are now presented to demonstrate some of the fundamental features of near-source ground motions. Figure 1 shows the geometry of the fault and a portion of the finite element mesh of tetrahedral elements. Each element in the figure represents 64 smaller tetrahedra which gives a typical node spacing on the ground surface of 170 m. This spacing is required to accommodate the shear wave speed of 0.7 km/sec at the surface and a frequency resolution up to 0.5 Hz, while the spacing at the base is 750 m where the shear wave speed is 3.8 km/sec. A total of 5.1 million degrees of freedom are present.

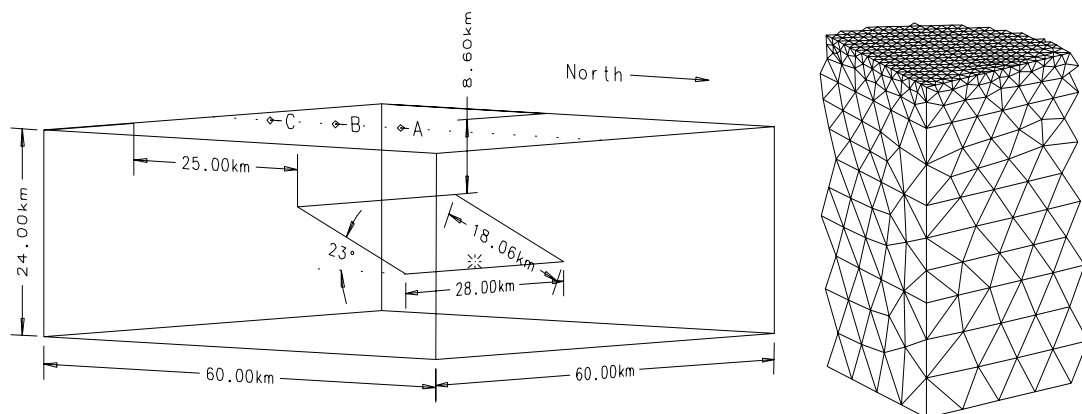


Figure 1: Diagram of domain and fault geometry and an edge of the course mesh.

The hypocenter is marked in Figure 1 as a small star. From here the rupture front is specified to propagate out radially with a velocity of 2.7 km/sec, which is 80% of the local shear wave speed. As the rupture front arrives at a point on the fault, slip begins and follows an exponential time function [1] which ultimately produces an offset of two meters at a rake of 105° . With this time function, 80% of the total slip at a point takes place in the first 1.5 sec, and the peak slip velocity is 147 cm/sec. The uniform spatial distribution of the slip is a simplification and is used here for demonstration purposes. The moment magnitude for this scenario earthquake is M_W 7.0.

Figure 2 and Figure 3 present contours of velocity on a vertical north-south section through the centerline of the fault and on the ground surface. The building up of the wave ahead of the rupture and the directivity effect are clearly evident. The plot at the ground surface shows a double velocity peak which is the forward and reverse motion of the near-source shear wave. The area swept out by this wave, though limited to the region south of the fault, is still quite significant in

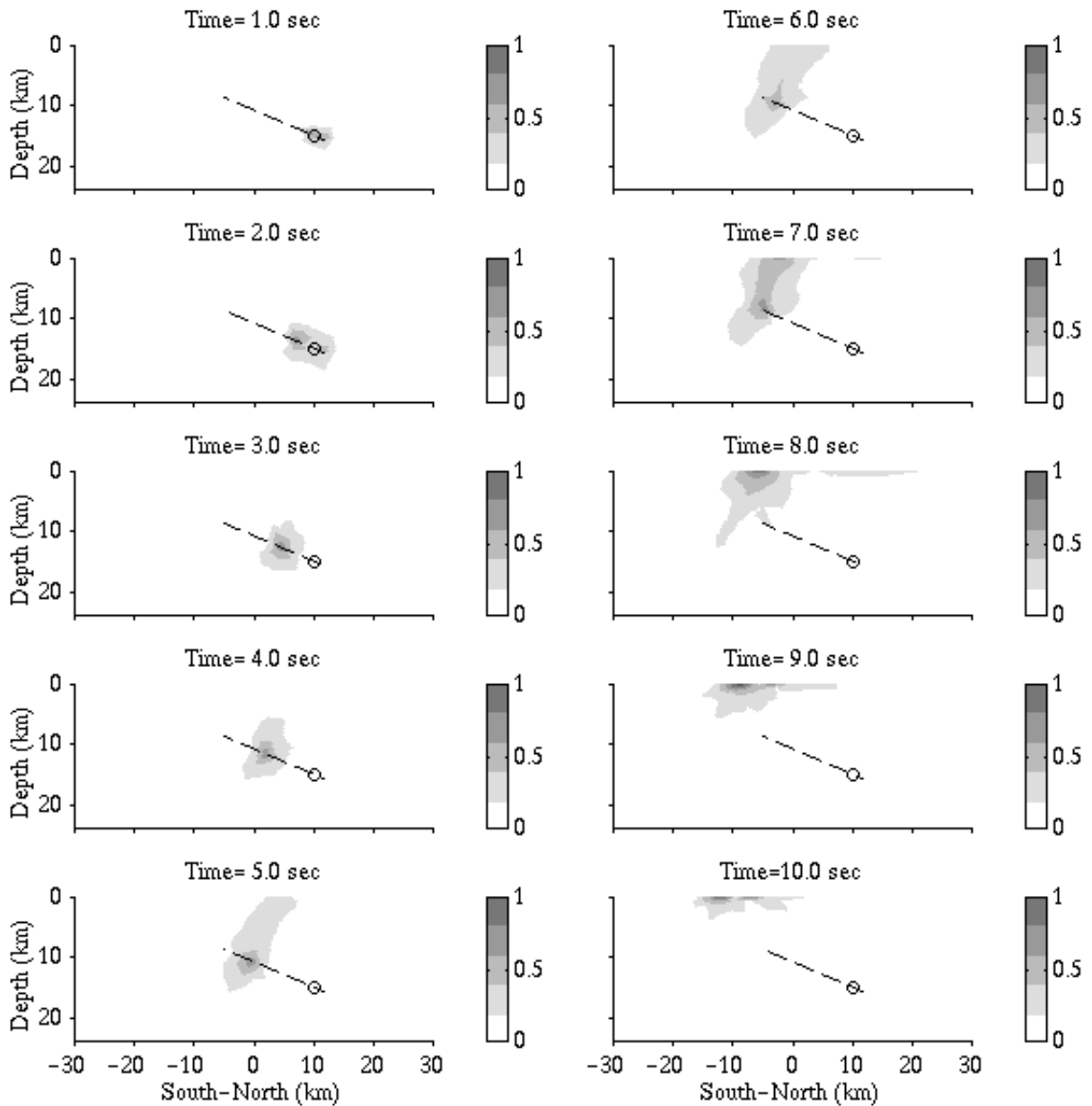


Figure 2: Velocity magnitude (m/sec) snapshots for a north-south slice at the fault centerline.

extent.

The ground motions for three sites located along the centerline of the fault are shown in Figure 4. The location with the maximum velocity along this line is site B located 6 km south of the top edge of the fault. Sites A and C lie 10 km north and south of site B, respectively. For site B the maximum horizontal velocity of 100 cm/sec is not surprising considering that higher velocities have been observed in smaller earthquakes such as the M_W 6.7 Northridge event. However, the maximum horizontal displacement of 140 cm greatly exceeds any displacement during the

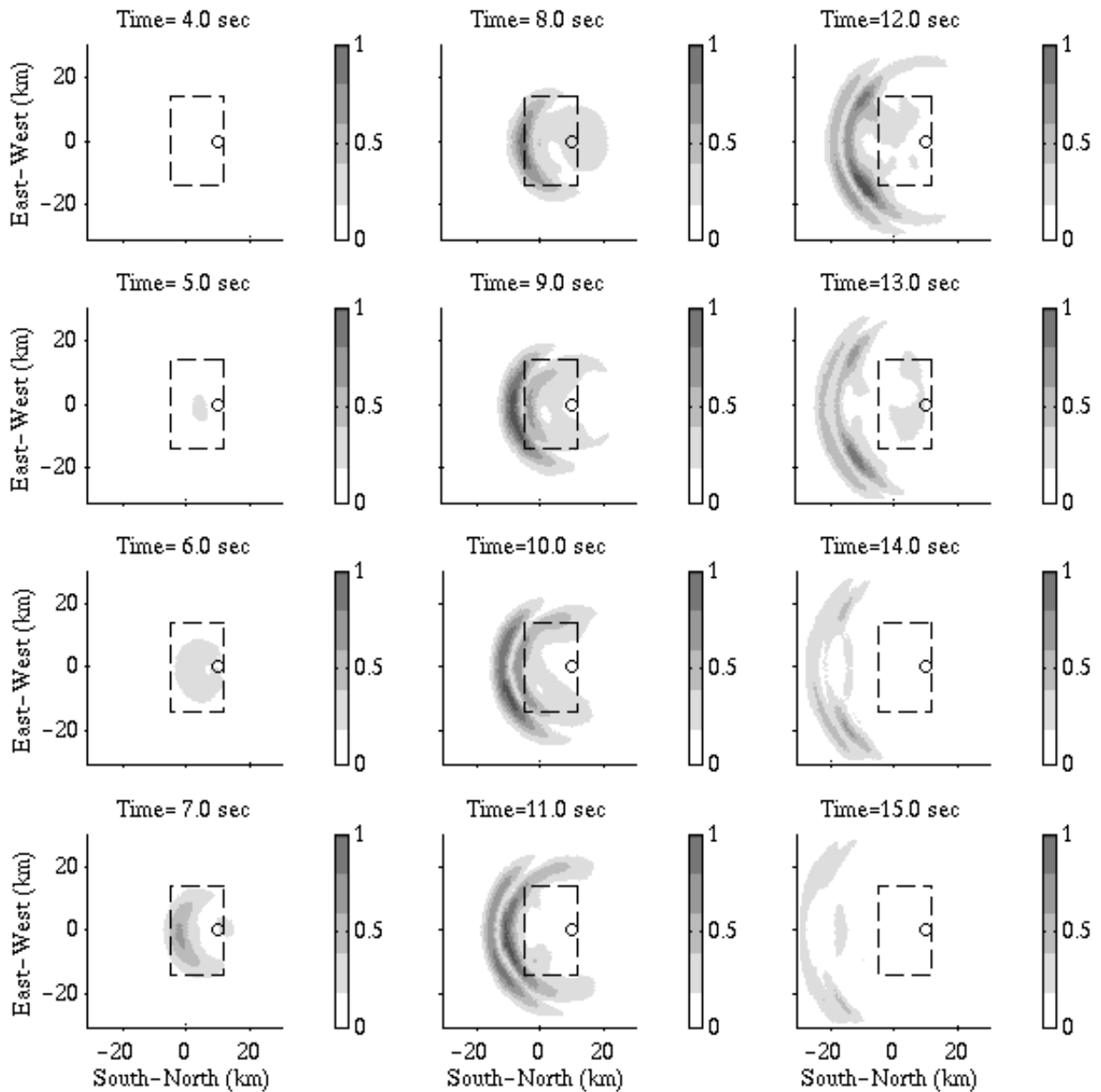


Figure 3: Velocity magnitude (m/sec) snapshots on the ground surface.

Northridge event, and this demonstrates the ability of bigger earthquakes to produce large ground displacements. It is also possible the uniform slip distribution somewhat exaggerates the amplitude at site B, emphasizing the importance of understanding more about the fault rupture process so that realistic slip histories may be specified. Figure 4 shows that at site A the vertical component of motion, which is associated mostly with the residual displacement, is significant with a maximum velocity of 41 cm/sec and a maximum displacement of 97 cm.

In summary, ground motions generated by the numerical simulation exhibit the near-source

effects of large, rapid displacements and directivity. The reversing fault-normal component is potentially the most damaging. Additionally, one should expect the amplitude of the ground displacement to increase significantly with earthquake magnitude even for a seemingly moderate increase in magnitude from M_W 6.7 to M_W 7.0.

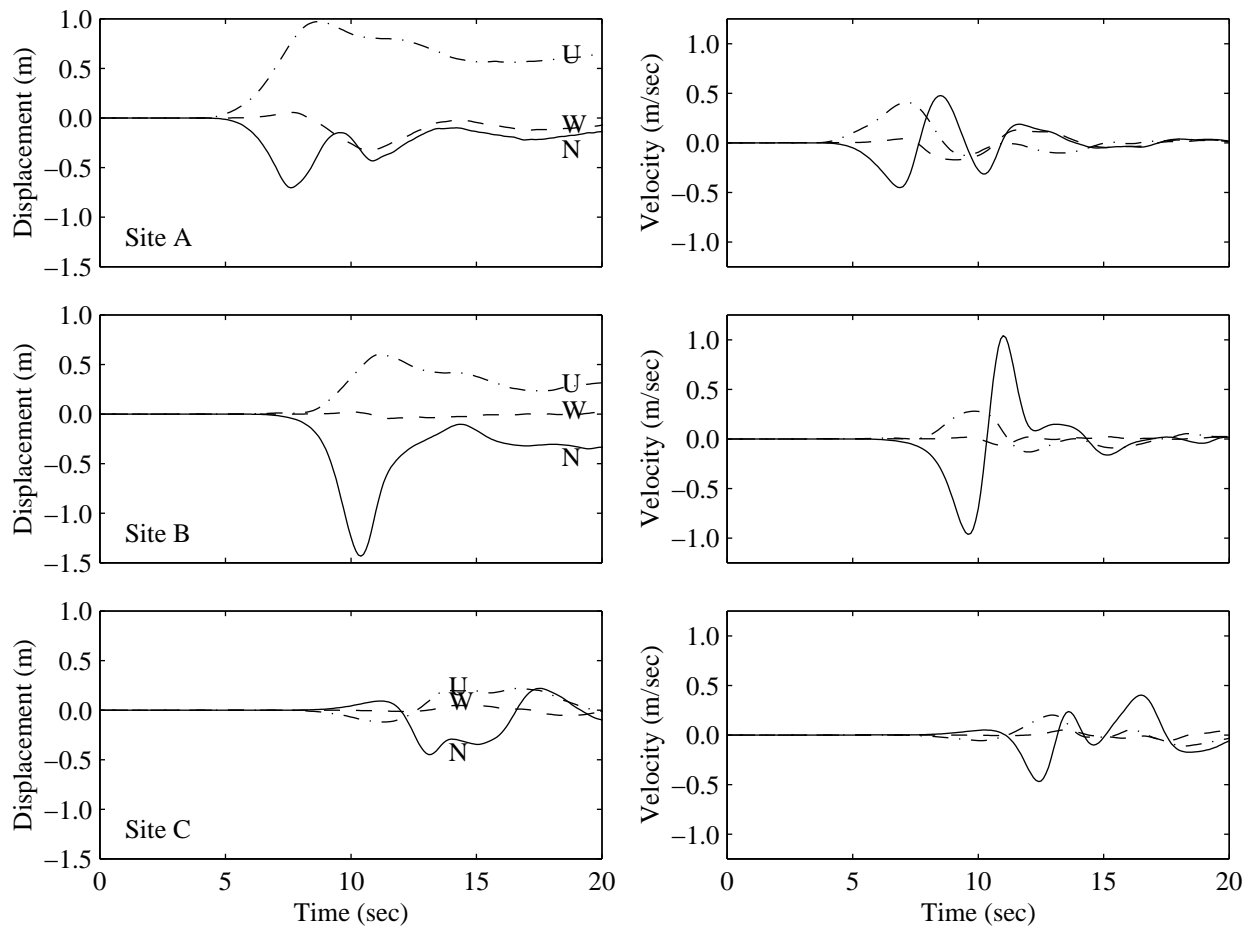


Figure 4: Displacement and velocity time histories at three sites on the ground surface.

Note: The computations for the simulation described above were carried out using 256 processors on one of Caltech's parallel computers. The total run time was 1.7 hours. Current capability at Caltech permits increasing the number of degrees of freedom by more than an order of magnitude. The work reported here is part of a project on earthquake ground motion simulation being carried out by the authors and Prof. Thomas Heaton of Caltech.

2 Structural Response

As seen in section 1, the simulated horizontal displacement of the ground from the thrust earthquake is dominated by a single, large, rapid pulse. This displacement contains a forward phase and a reversing phase, and an idealized version is depicted in Figure 5(a). T_P is the duration of the dis-

placement pulse; relations among peak acceleration, velocity and displacement are as shown. This motion, which can also represent near-source motion in the direction normal to the fault during a strike-slip earthquake, is used here in a study of the nonlinear response of a single-degree-of-freedom oscillator.

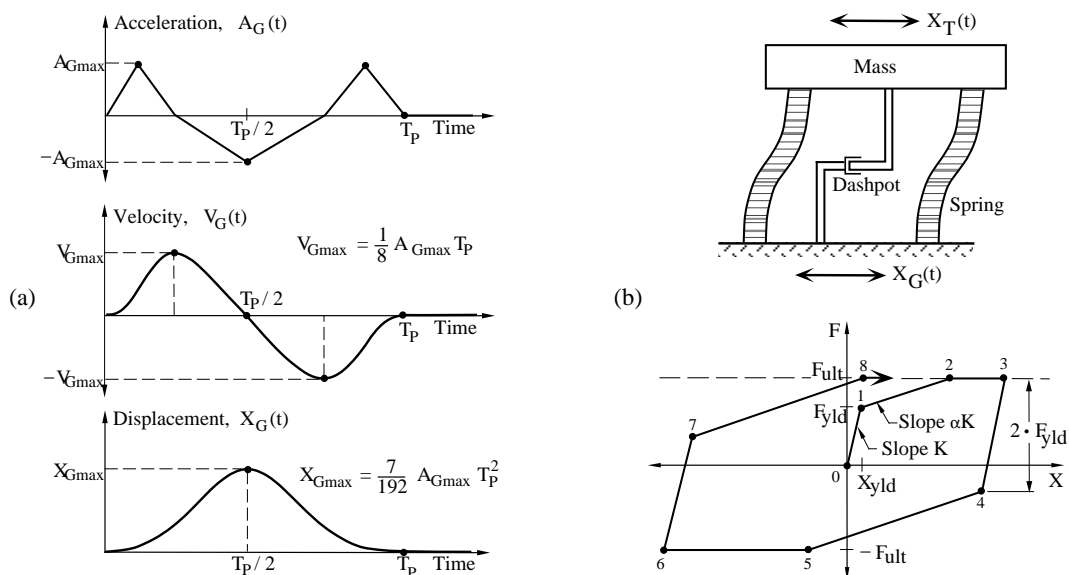


Figure 5: (a) Idealized displacement pulse ground motion. (b) Single degree of freedom oscillator and force-deflection curve for spring.

The oscillator shown in Figure 5(b) has mass M and absolute displacement $X_T(t)$ which is the sum of the ground displacement, $X_G(t)$, and the relative displacement, $X(t)$. The spring stiffness is trilinear (Figure 5(b)) with a secondary stiffness αK equal to 15% of the initial stiffness K . The ultimate strength F_{ult} exceeds the yield strength F_{yld} by 30%. The dashpot provides viscous damping at 5% of critical except the dashpot force is capped at 10% of F_{ult} . This simple system is intended mainly as a tool for characterizing the ground motion; the actual response of a bridge is more complicated due to P- Δ effects, structural degradation, soil-foundation interaction, and multiple degrees of freedom.

Properties of the oscillator are chosen based on Caltrans design criteria [7]: the 0.7 g ARS spectrum for 10 to 80 feet of alluvium, and Z for well-confined, ductile, single-column bents. The normalized strength F_{yld}/Mg is set equal to the ARS value divided by Z and is a function of the period T_1 of the oscillator (see Figure 9, Caltrans curve).

Ductility and strength demands are assessed using two idealized ground motions based on Figure 5(a) and one actual recorded ground motion. The two idealized motions are denoted P75 ($T_p = 2$ sec, $D_{Gmax} = 75$ cm, $A_{Gmax} = 514$ cm/sec²) and P150 ($T_p = 4$ sec, $D_{Gmax} = 150$ cm, $A_{Gmax} = 257$ cm/sec²), and both have the same $V_{Gmax} = 129$ cm/sec. P75 and P150 represent fairly severe motions, but are by no means upper bounds on what is possible. Since P75 and P150 lack high-frequency content, the free-field record at the Olive View Hospital from the 1994 M_W 6.7 Northridge earthquake (denoted by OVH) is chosen as a reference. This record is rich in high

frequencies and contains some near-source effects from a moderate earthquake. OVH has peak acceleration, velocity and displacement of 818 cm/sec^2 , 131 cm/sec and 31 cm , respectively, and has been rotated in the horizontal plane to maximize the peak-to-peak velocity.

Ductility demand, shown in Figure 6, is defined as the ratio of $\max|X_T(t)|$ to X_{yld} . Two of the ground motions, P75 and, especially, OVH, show high demands at low periods, because their accelerations are large enough to yield the oscillator spring, and the denominator X_{yld} in the ductility demand calculation goes to zero as the period T_1 approaches zero. This is typical for ground motions containing high accelerations but may not be as serious as the plot suggests, because the actual amount of plastic deformation is small. More serious are the large ductility demands at the longer periods which are produced by P75 in the intermediate period range and by P150 in the longer period range. These indicate considerable potential for damage, and an oscillator whose period T_1 is about half the period T_P of the ground pulse is most susceptible.

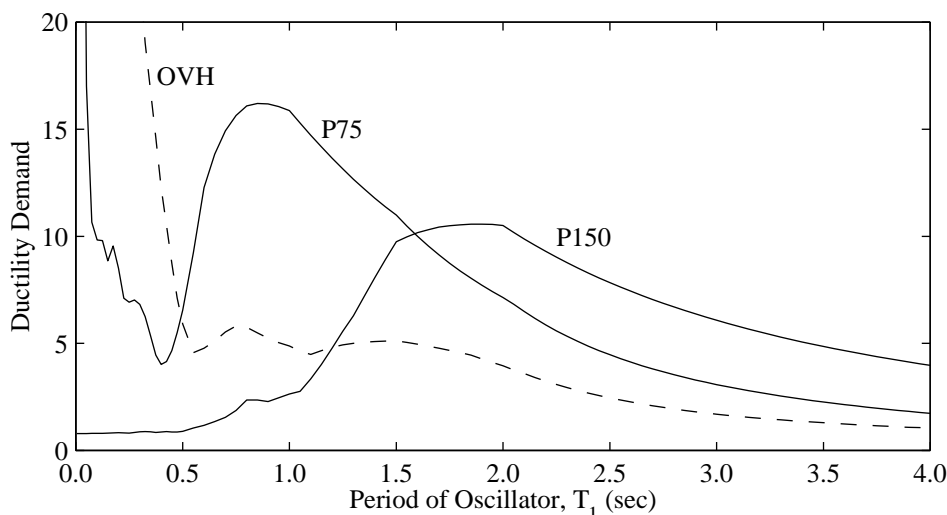


Figure 6: Ductility demand for Caltrans design strength under three ground motions.

Figure 7 contains the displacement history of the P75 ground motion and that of the oscillator with $T_1 = 0.9 \text{ sec}$ which has the peak ductility demand. The large nonlinear response of this oscillator can be explained as follows. During the entire forward motion of the ground, the ground stays ahead of the mass and so does positive work on it, increasing its kinetic energy. This kinetic energy attains a maximum at the instant when the mass catches up to the ground, which from Figure 7 is also the instant when the ground reverses its direction. The situation then becomes one of the mass moving forward as the ground reverses, resulting in a large excursion of the spring into the nonlinear range. To experience the full effect of the ground displacement pulse, the mass must catch up to the ground just when the ground is beginning to reverse its direction. If the spring remains elastic, this timing would occur for the oscillator whose period T_1 equals T_P . But yielding in the spring during the forward motion of the ground delays the progress of the mass, and so the critical timing occurs for a stiffer oscillator; in this case the one with a period $T_1 = 0.9 \text{ sec}$.

Figure 8 shows ductility demands recomputed with the strength of the spring increased by a

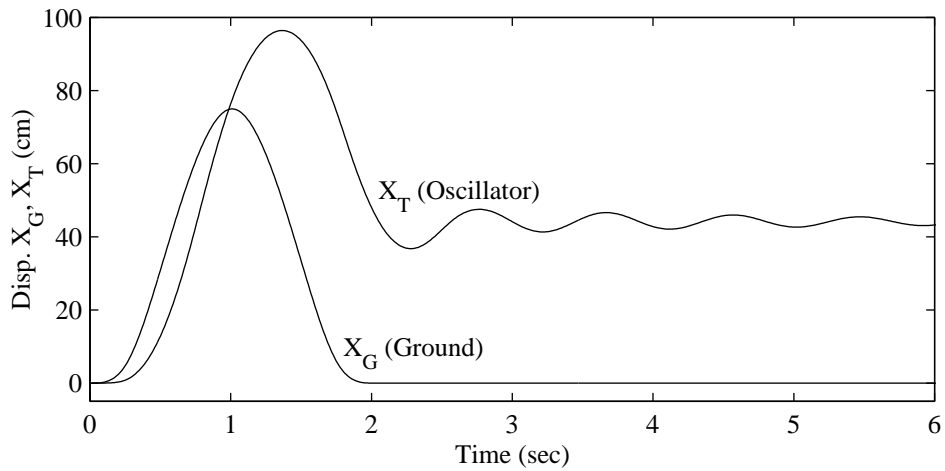


Figure 7: Displacement time histories for the P75 pulse: X_G of the ground and X_T of the oscillator with fundamental period $T_1 = 0.9$ sec.

factor of 1.5, because the ductility demands in Figure 6 are so large. Although substantial reduction occurs in the ductility demands, much of it results from X_{yld} being larger; nevertheless, they are still quite high.

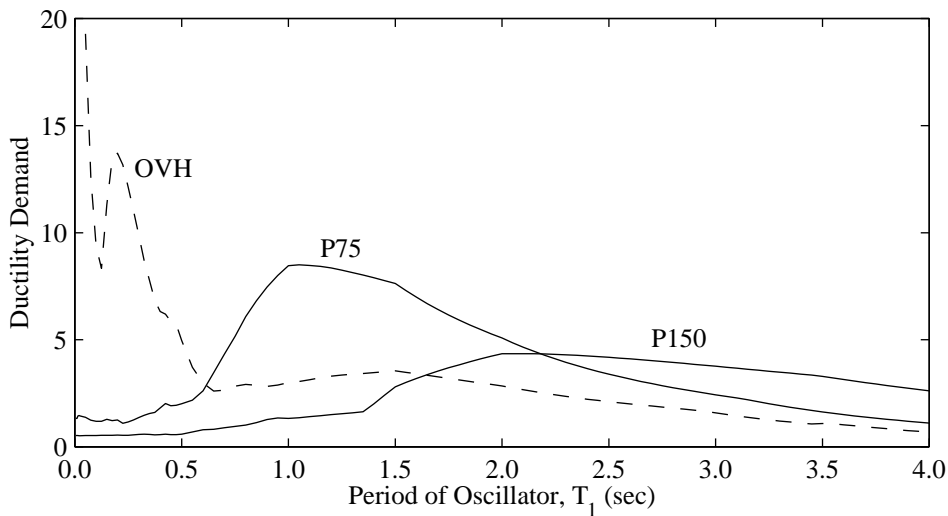


Figure 8: Ductility demand for 1.5 times the Caltrans design strength under three ground motions.

Figure 9 presents the strength F_{yld}/Mg necessary to limit the ductility demand to four. For reference, the Caltrans design strength is plotted (ARS spectrum and Z given earlier) as well as the ATC-32 [8] design strength (0.7 g ARS spectrum for soil type C and $M = 7.25$; Z for full ductility structures with well-confined columns). For strength demand, like ductility demand, OVH controls in the short period range, P75 in the intermediate period range, and P150 in the longer period range. The ATC-32 strength adequately meets the OVH strength demand, but it and the Caltrans strength fall considerably below the P75 and P150 strength demands at moderate and longer periods.

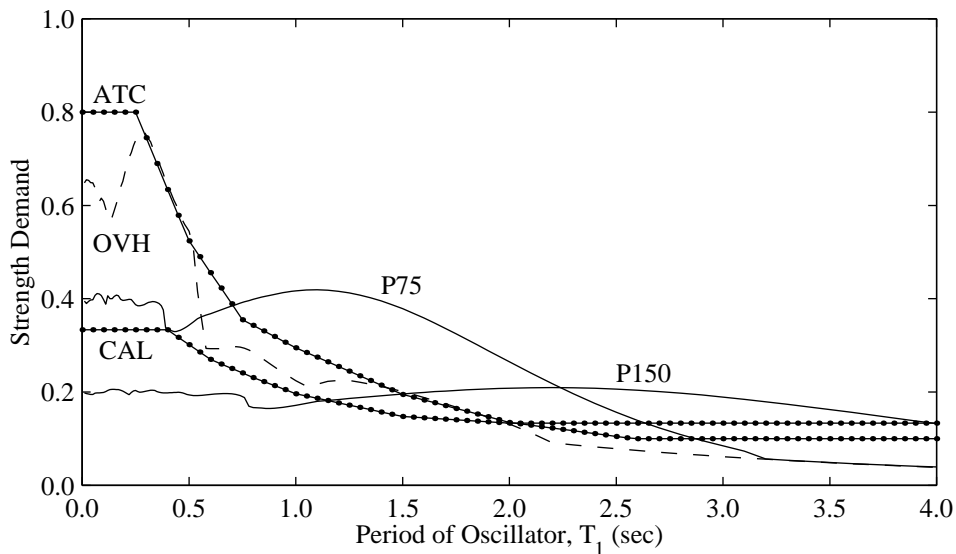


Figure 9: Strength required to limit ductility demand to four under three ground motions. CAL and ATC are Caltrans and ATC-32 design strengths as discussed in text.

To investigate this further, Figure 10 presents strength demand envelopes for suites of pulses of the type shown in Figure 5(a). The $V_{Gmax} = 129$ cm/sec curve is an envelope of strength demands for pulses (including P75 and P150) having this maximum velocity and covering the entire period range T_p , except at shorter periods where A_{Gmax} would exceed 0.8 g, the ground motion amplitude is reduced to this level. The $V_{Gmax} = 100$ cm/sec and 70 cm/sec curves are similar envelopes for ground motion pulses whose amplitudes exceed neither these maximum velocities nor $A_{Gmax} = 0.8$ g. The ATC-32 strength mostly meets the demand for the $V_{Gmax} = 70$ cm/sec ground motions, but falls considerably below that for the higher velocity pulses at moderate and longer periods. The Caltrans strength falls even further below except at the longer periods.

In summary, near-source displacement pulses of the type considered here would impose large ductility demands on currently designed bridges over a wide period range, even bridges with fundamental periods below one second. The reversing displacement pulse can cause severe damage by propelling the structure forward and then reversing direction. Strengths required to limit ductility demand to four can be very high and uneconomical, which presents a dilemma for bridge designers who must also consider that the probability of experiencing strong near-source effects in the lifetime of a bridge may be small.

References

- [1] J.F. Hall, T.H. Heaton, M.W. Halling, and D.J. Wald. Near-source ground motion and its effects on flexible buildings. *Earthquake Spectra*, 11(4):569–605, November 1995.
- [2] W.D. Iwan and X.D. Chen. Important near-field ground motion data from the Landers earthquake. In *Proceedings, 10th European Conference on Earthquake Engineering*, 1994.

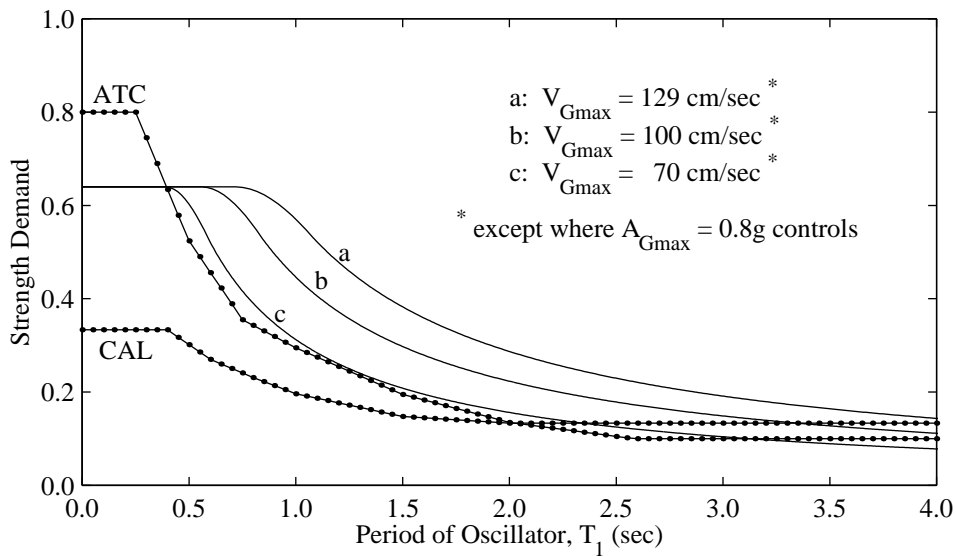


Figure 10: Envelopes of strength required to limit the ductility demand to four under three suites of ground pulses with different peak velocities.

- [3] K.B. Olsen and R.J. Archuleta. 3-dimensional simulation of earthquakes on the Los-Angeles fault system. *Bull. of the Seism. Soc. of Amer.*, 86(3):575–596, 1996.
- [4] R.W. Graves. Simulating seismic-wave propagation in 3D elastic media using staggered-grid finite-differences. *Bull. of the Seism. Soc. of Amer.*, 86(4):1091–1106, Aug. 1996.
- [5] J. Bielak. The quake project. Technical report, Carnegie Mellon University, <http://www.cs.cmu.edu/afs/cs/project/quake/public/www/quake.html>, 1998.
- [6] E. Fukuyama and R. Madariaga. Rupture dynamics of a planar fault in a 3D elastic medium: Rate- and slip- weakening friction. *Bull. of the Seism. Soc. of Amer.*, 88(1):1–17, February 1998.
- [7] Seismic design references. Technical report, California Department of Transportation, 1990.
- [8] R.V. Nutt. ATC-32: Improved seismic design criteria for California bridges: Provisional recommendations. Technical report, Applied Technology Council, 1996.